Chemical Physics 601 (2026) 112952

Contents lists available at ScienceDirect

Chemical Physics

journal homepage: www.elsevier.com/locate/chemphys

Ecofriendly high-performance low-cost $Cu_2ZnSnSe_4$ solar cells: Experimental characterization and SCAPS-1D simulation

Feriha Afrah Boukhelkhal [a], Naceur Selmane [a,*], Ali Cheknane [a,*], Moustafa Noureddine [b], Abdelhalim Zoukel [c], Nilgun Baydogan [d], Büşra Günalan [d], Hikmat S. Hilal [e,*]

[a] Laboratoire Matériaux, Systèmes Énergétiques, Énergies Renouvelables et gestion de l'Énergie (LMSEERGE), Ammar Telidji University, Martyrs Boulevard BP37G, Laghouat 03000, Algeria
[b] Process Engineering Laboratory, Ammar Telidji University, Martyrs Boulevard BP37G, Laghouat 03000, Algeria
[c] Physical-Chemistry Materials Laboratory, Ammar Telidji University, Martyrs Boulevard BP37G, Laghouat 03000, Algeria
[d] Istanbul Technical University, Energy Institute, Ayazaga Campus-Maslak, Istanbul, Turkey
[e] SSERL, Department of Chemistry, Faculty of Sciences, An-Najah National University, Nablus P400, Palestine

ARTICLE INFO

Keywords:
Sol-gel
CZTSe films
Absorber-layer thickness
Doping concentration
SCAPS-1D

ABSTRACT

$Cu_2ZnSnSe_4$ (CZTSe) is a promising low-cost and ecofriendly p-type semiconductor for solar cells. However, CZTSe solar cells are have shortcomings, as they typically involve hazardous CdS-buffer layers. Costly dopant elements Ag and/or Ge are also normally used. This study aims at producing efficient, ecofriendly and low-cost solar cells. The Cd-, Ag- and Ge-free configuration metal/$MoSe_2$/CZTSe/ZnSe/i-ZnO/ZnO-Al/metal is proposed. CZTSe film is prepared by the facile and low-cost sol-gel method, and characterized by elemental analysis, optical-absorption spectra, surface morphology, surface profiling and wettability. The cell is simulated by SCAPS-1D. Optimal CZTSe-layer thickness is 2.5 μm with optimized doping concentration 5×10^{16} cm^{-3}. With these parameters, the cell exhibits an open-circuit potential 0.56 V, a short-circuit potential 47.33 mA/cm^2 and a fill factor 73.82 %. With a cell conversion efficiency 19.5 %, the proposed cell outperforms earlier CZTSe cells in terms of cost and environmental friendliness. This opens new research inroads toward improved CZTSe-based solar cells.

1. Introduction

$Cu_2ZnSnSe_4$, CZTSe, has emerged as a promising semiconductor absorber material for thin-film photovoltaics, due to its special opto-electronic characteristics and environmentally benign composition. $Cu_2ZnSnSe_4$ has a wurtzite hexagonal closely-packed structure, in resemblance to that of Cu_2ZnSnS_4 [1],[2]. As a member of the kesterite family, CZTSe possesses a direct bandgap ranging 1.0–1.1 eV [2–4], which is nearly ideal for single junction solar cells, with reference to Shockley-Queisser limitations. The material demonstrates a very high absorption coefficient of $>10^4$ cm^{-1} [5–9], enabling efficient light absorption in thin films of the order of micrometer thicknesses. This characteristic, combined with its good carrier mobility, makes the p-type semiconductor CZTSe particularly attractive in photovoltaics. Kasterite abundant and ecofriendly constituent elements present a significant advantage over other competing thin-film materials such as the costly $CuInGaSe_2$ (CIGS) [10–12] or the hazardous CdTe [13]. The material demonstrates sound thermal stability [14] and radiation resistance, properties that are crucial for long-term device operation. Furthermore, CZTSe maintains good electronic properties even when processed using simple fabrication methods [11–13]. Both solution-based techniques and vacuum deposition methods are known [13], [14]. Recently, CZTSe-based solar cells were reported with sound performance. Typically, the cells involved CZTSe absorber layer, together with molybdenum metal (Mo) as the back-contact, n-CdS as the buffer layer material, and a transparent-conductive oxide (TCO) as the front contact.

In CZTSe-based solar cells, buffer layers are key factors that control overall optoelectronic performances. Both material type and layer thickness influence light absorption [15], interface recombination and carrier transport efficiency. Traditionally, CdS has been employed due to its favorable band alignment (small conduction band spike) and ability to reduce surface recombination. However, cadmium poses serious environmental and health concerns and should be avoided whenever

* Corresponding authors.
E-mail addresses: n.selmane@lagh-univ.dz (N. Selmane), a.cheknane@lagh-univ.dz (A. Cheknane), hshilal@najah.edu (H.S. Hilal).

https://doi.org/10.1016/j.chemphys.2025.112952
Received 2 August 2025; Received in revised form 20 September 2025; Accepted 22 September 2025
Available online 23 September 2025

possible. Moreover, the CZTSe/CdS junctions were reported to have low stability. Buffer layer thickness also affects CZTSe solar cell performance. Using thick buffer layers, which are placed above the absorber layer, Fig. 1, lowers the absorber layer absorption. Therefore, efforts are always made to use thin buffer layers [16,17]. In the present work, we have used a thin layer (0.05 μm) of ZnSe to replace the hazardous CdS buffer, vide infra.

The current recorded efficiency for pure CZTSe solar cells stands at 12.6 % [18],[19], while devices incorporating sulfur to form CZTSSe have reached slightly higher efficiencies of 13.0 % [20]. These performance metrics, while still below the theoretical limit, demonstrate the potential of this material system. The efficiency limitations in CZTSe devices primarily stem from voltage deficits caused by band tailing and deep-level defects. Research has shown that these issues can be mitigated through careful control of stoichiometry, with particular attention to the Zn/Sn or Cu/(Zn + Sn) ratios [21]. Alkali doping, particularly with sodium or potassium, has proven effective in passivating grain boundaries and improving device performance [22]. Interface engineering, including the development of alternative materials for buffer layers, such as Zn(O,S) or In_2S_3, has also contributed to recent efficiency improvements [23]. Ongoing research directions for CZTSe photovoltaics include the development of graded bandgap structures, improved defect passivation strategies, and the integration of CZTSe into tandem cell configurations. The material versatility also makes it suitable for emerging applications such as flexible and semi-transparent photovoltaics [24]. With continued optimization of material properties and device architectures, CZTSe-based solar cells should become highly competitive in thin-film photovoltaics.

To prepare CZTSe films, several methods were reported, including physical vapor deposition (PVD) [25],[26], chemical bath deposition (CBD) [27],[28–30], co-evaporation, nanoparticle ink-based techniques and the sol-gel method [31],[32]. Among these, the sol-gel is an efficient method due to its ease of control, low cost and the relatively mild required preparation conditions. It also enables the fabrication of homogeneous thin films over wide areas, making it applicable in industrial-scale applications. Moreover, this technique allows for molecular-level control of the chemical composition, which improves the crystalline quality and lowers structural defects. Literature demonstrated that the sol-gel method enhances the electrical and optical properties of CZTSe layers, thus improving their performance in photovoltaic devices [33].

The present study is divided into two major parts. Firstly, the CZTSe material is synthesized by sol-gel method and its physical properties are thoroughly characterized. Secondly, a solar cell based on CZTSe is designed and analyzed to evaluate its photovoltaic performance. The complete cell configuration is metal/$MoSe_2$/CZTSe/ZnSe/i-ZnO/ZnO-Al/metal, which was not earlier reported, to our knowledge. The n-ZnSe layer is used here to replace the commonly used hazardous n-CdS buffer layer described earlier [34],[35]. With CdS buffer layer, the CZTSe solar cells reached conversion efficiency values ~18 % or lower. The present configuration aims at providing higher conversion efficiency while avoiding the hazardous CdS. Costly doping elements, such as Ge and Ge, which were described earlier [36],[37], are avoided here to lower the cell production costs. The new proposed solar cell will be assessed here for the first time, in comparison with earlier reported ones, to highlight its potential for future solar cells.

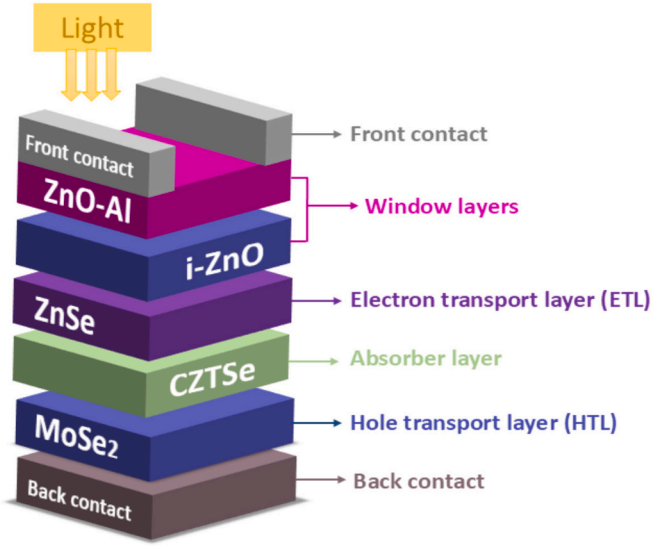

Fig. 1. A schematic for the new CZTSe-based solar cell.

2. Materials and methods

2.1. Common materials

Most pure form chemicals, such as selenium, terpineol, ethyl cellulose and other common solvents have been acquired from Sigma-Aldrich. Microscopic glass substrates (Objekttrager 76× 26 mm/3 × 1 in.) are from ISO LAB, GERMANY,

2.2. Equipment

KSV Dip Coater (KSV instruments Ltd) with program control (KSV NIMA DC) is used for film preparation by dip coating. A four-digit analytical Mettler Toledo AB54-S/FACT is used for weighting. A PROTHERM Alser S.A furnace is used for annealing. For surface profilometry, a DEKTAK-6 M SURFACE PROFILOMETER with 3 mg load to the surface, is used. For the contact angle measurement, a KSV CAM 200 CONTACT ANGLE METER, with a drop (5 μL) of distilled water onto the sample surface, is used. An MEB Quattro S de Thermo fisher scientific (Holand) machine has been used for scanning electronic microscopy (SEM) measurement. For electronic absorption spectral measurement a 1800 Shimadzu spectrophotometer is used. An Edx Octane elite (EDAX), USA, is used to measure energy dispersive spectra (EDS).

2.3. Films preparation

Microscopic glass substrates (76 mm × 26 mm) are properly cleaned by standard methods with acetone, ethanol and distilled water for 15 min. All laboratory glassware are properly cleaned prior to use. Individual precursor solutions have been prepared as follows:

- $CuCl_2{\cdot}2H_2O$ (1.023 g, 0.006 mol) in ethanol (20 mL) with 3.0 mL of diethanolamine (DEA) added to it to prepare Cu^{2+} (M = 0.261 mol/L) solution.
- $Zn(C_4H_4O_6){\cdot}2H_2O$ (0.439 g, 0.0018 mol) in ethanol (20 mL) with 0.12 mL of DEA added to it to prepare Zn^{2+} (M = 0.089 mol/L) solution.
- $SnCl_2$ (0.676 g, 0.0036 mol) in ethanol (30 mL) with a suitable amount of DEA added, to prepare Sn^{2+} (M = 0.119 mol/L) solution.;
- Selenium (0.194 g, 0.0025 mol) in a solution of terpineol (7.520 g), ethyl cellulose (0.375 g) and ethanol (10 mL) with the resulting Se solution concentration of M = 0.246 mol/L.

After the individual solutions are prepared, solutions of Cu^{2+} (4 mL), Zn^{2+} (2 mL), Sn^{2+} (2 mL) and Se (8 mL) are mixed and homogenized by magnetic stirring for 10 min. The resulting solution is then used for film deposition on the KSV dip coater, controlled by the KSV NIMA software, under dipping speed of 200 mm/min for 20 s. Four glass substrates are used, each coated with ten consecutive layers. After each cycle, the sample is dried at 160 °C for 10 min to allow solvent evaporation and improve film formation. Finally, the coated substrates are subjected to thermal annealing for 1 h at 500 °C, in a furnace under air to improve the

resulting CZTSe thin-films crystallinity.

2.4. Characterization

The surface morphology for CZTSe ($Cu_2ZnSnSe_4$) material and grain distribution are examined using SEM. The elemental composition and stoichiometry are analyzed through EDX spectra. Absorption coefficient has been calculated from the electronic-absorption spectra, which are measured for the CZTSe film deposited onto glass. A naked glass slide is used as a background control. Furthermore, the surface wettability has been studied using contact angle as described above. The topographical features are explored through surface profile analysis.

2.5. SCAPS numerical simulation

In this part, numerical simulations are conducted using the Solar-Cell Capacitance Simulator–1 Dimension (SCAPS-1D), Version 3309. This is a 1-dimensional software tool, developed by Ghent University, which was widely used for modeling thin-film photovoltaic devices [38–40]. SCAPS-1D enables the analysis of device performance by solving the coupled semiconductor equations that describe charge generation, transport and recombination under steady-state or transient conditions. The simulation relies on the self-consistent solution of three fundamental equations, Poisson & Continuity Eqs. (1) and (2a, 2b), in addition to the transport of electron and hole charge carrier Eqs. (3a, 3b, 3c) [41].

$$\frac{\partial^2}{\partial x}\varphi(x) = \frac{q}{\varepsilon_0 \varepsilon_r}\left(p(x) - n(x) + N_D + N_A + \rho_p + \rho_n\right) \tag{1}$$

$$\frac{\partial J_P}{\partial x} - R_P + G_P = \frac{\partial P}{\partial x} \tag{2a}$$

$$\frac{\partial J_n}{\partial x} - R_n + G_n = \frac{\partial n}{\partial t} \tag{2b}$$

$$J_n = q\mu_n E_n + qD_n d_n \tag{3a}$$

$$J_P = q\mu_P E_P + qD_P d_P \tag{3b}$$

$$D_P = \frac{KT}{q}\mu_P, D_n = \frac{KT}{q}\mu_n \tag{3c}$$

where φ is electrostatic potential, while ρ is charge density in-space, and E describes electric field. ε_0 and $\varepsilon_r$are relative-permittivity values in vacuum and material, respectively, n and p are concentrations of free electrons and holes, respectively. N_A and N_D describe acceptor and donor concentrations. μ_n & μ_P are mobilities of electrons and holes, respectively. G_n & G_P denote optical generation rates. R_n & R_P denote the recombination rates, while q represents charge. D_n and D_P describe electron & hole diffusion coefficients, respectively. K is Boltzmann constant, while T is temperature (K).

The proposed solar cell structure ZnO:Al/ZnO(i)/ZnSe(ETL)/CZTSe/$MoSe_2$(HTL) involves several integrated layers that work synergistically to efficiently convert light into electricity, with each layer playing specific electronic and optical roles. The structure begins with the ZnO:Al layer (also known as AZO), which serves as a transparent conducting oxide (TCO) [42–45], combining high electrical conductivity with excellent optical transmittance [46]. It also allows photons to reach the active layers while efficiently collecting electrons. Next is the intrinsic ZnO (ZnO(i)) layer, which acts as a buffer to decrease interface defects and improve band alignment, thus minimizing surface recombination and enhancing charge collection efficiency [47]. Following this is the ZnSe layer, used as an electron transport material (ETL). It has a wider bandgap (2.7 eV) than CZTSe. The ZnSe layer thickness was optimized at 0.05 μm, which represents the ideal value to ensure high light transmittance while maintaining interface quality for efficient charge transport. This ensures high transparency in the visible spectrum and minimizes parasitic absorption, which allows more photons at the absorber layer [48]. Moreover, ZnSe furnishes sound good band alignment with CZTSe, facilitating efficient electron extraction and transport while acting as an effective barrier against hole backflow. It is also responsible for extracting electrons from the absorber and transporting them to the TCO while blocking holes, ensuring selective charge extraction [49]. The new configuration is thus anticipated to exhibit high performance. The selection of ZnSe, instead of CdS, as electron-transport layer (ETL) here is also motivated by environmental and health considerations. While CdS has traditionally been used due to its favorable band alignment and well-established processing techniques, it contains the hazardous cadmium, as described above. By replacing CdS with ZnSe, the device aligns better with sustainable green technology principles, making it more suitable for large-scale deployment. These are the reasons for using ZnSe as a buffer layer on one hand and as an electron transfer layer (ETL) on the other hand, as a replacement for CdS.

The central absorber layer, CZTSe ($Cu_2ZnSnSe_4$), is the core of the device, with a near-optimal bandgap (1.0 eV) that enables efficient absorption through a wide solar spectral range. The layer is free of costly dopants such as Ge or Ag. Under illumination, this layer generates electron and hole pairs that are can be separated by virtue of the built-in electric field.

At the rear side lies the $MoSe_2$ layer, typically formed from a thermal reaction between molybdenum and selenium during annealing. This layer behaves as a hole-transport layer (HTL) and improves ohmic contact with the back electrode. It also forms an energy barrier that prevents electron leakage toward the back contact, thereby improving hole selectivity and reducing losses. $MoSe_2$ is an ecofriendly alternative to several commonly used hazardous materials such as CuI, CuSCN and NiO_x in solar cells. It offers favorable energy level alignment with the absorber layer, which efficientiy facilitates hole extraction and transport while minimizing interfacial recombination [50],[51]. Moreover, $MoSe_2$ is a chemically stable material. These are the reasons for using $MoSe_2$ as a THL here [52].

The abundant recyclable aluminum (Al) is used here as the metal contact for more than one reason. Firstly it is less costly than other special metals such as Au which was described in literature [53]. Secondly, it is less hazardous than other heavy metals like Ni. Furthermore, Al possesses high electrical conductivity and forms effective contacts with semiconductor layers, thereby supporting efficient charge extraction without compromising device performance. Al has been described in solar cell systems in literature [54].

The influence of both shunt resistance (Rsh) and series resistance (Rs), on the photovoltaic performance of the solar cell can be explained quantitatively and physically as follows [55],[56]:

Open-circuit otential (V_{OC}): V_{OC} is only slightly affected by *Rs* but is highly sensitive to *Rsh*. A low Rsh allows leakage currents through shunt paths, which significantly reduces V_{OC}. By contrast, an increase in *Rs* has little direct impact on V_{OC}.

Short-circuit current density (J_{SC}): When *Rs* is high, voltage drops occur across internal layers, which reduce the extracted current and lower the measured J_{SC}. Similarly, a low *Rsh* creates internal leakage pathways that divert part of the photogenerated current, also resulting in a reduction of J_{SC}.

Fill factor (*FF*): This parameter is highly sensitive to resistances. A high *Rs* causes bending of the current density vs. potential (*J-V*) plots and reduces *FF* due to ohmic voltage losses. Likewise, a low *Rsh* introduces curvature from the opposite side of the *J–V* plot (through leakage currents), which also decreases *FF*.

Power conversion efficiency (*PCE*): Since $PCE = V_{OC} \times J_{SC} \times FF/$ incident power (P_{in}), any degradation in one of these parameters due to *Rs* or *Rsh* directly decreases the overall efficiency. Even a moderate increase in *Rs* can significantly reduce efficiency at high currents, while a decrease in *Rsh* can cause severe leakage losses, especially at higher voltages.

A high *Rs* usually indicates poor electrical contact, excessive absorber thickness, or problems in the transport layers. This can be mitigated by improving conductivity or optimizing electrode interfaces. A low *Rsh* points to defects or shunting pathways (such as pinholes or secondary phases), requiring improvements in film quality and defect passivation. Practically, it is essential to maintain a low *Rs* and a high *Rsh* to achieve high V_{OC}, J_{SC}, and *FF*, and thus ensure high and stable *PCE*.

Altogether, this multi-layer architecture enables efficient light absorption, charge generation and separation and selective carrier transport, making it a promising design for safe, high-performance and low-cost solar cells. Fig. 1 illustrates the proposed solar cell structure, while Table 1 summarizes all physical parameter inputs in the simulation.

3. Results

3.1. Characterization results

The comprehensive characterizations furnish valuable insight into the quality and suitability of CZTSe absorber layer in solar cells, as described below. The results indicate the stability of the CZTSe layer after annealing at the stated temperature.

- SEM and EDAX

Fig. 2 presents the SEM micrographs measured for the CZTSe film at two different magnifications. The surface appears relatively clean, with small, irregular granular patterns. The fine particles are randomly distributed. In Figs. 2(a) and (b), there is a color change ranging from gray to light gray, indicating only slight variations in chemical or physical properties of the layer surface. However, the color changes suggest the presence of some localized corrosions or minor non-uniform depositions. Overall, the soundly homogeneous surface indicates favorable physical properties such as conductivity and corrosion resistance.

Fig. 3 shows the EDX spectrum for the CZTSe film. The elemental-analysis results are summarized in Table 2. The Table demonstrates the existence of all CZTSe elements in the film. Moreover, the expected stoichiometry $Cu_2ZnSnSe_4$ is soundly consistent with measured film composition. The experimental atomic ratios Cu:Zn:Sn:Se are approximately 23:13:11:52, respectively. These values are in congruence with the expected ratios 2:1:1:4 from the stoichimetry. The relatively high Se ratio is the reason for the p-type conductivity associated with the CZTSe film [57],[58].

Table 1
Physical parameters of materials used in simulations.

Parameters	ZnO-Al [87]	i-ZnO [88]	ZnSe	CZTSe	$MoSe_2$
Thickness (in μm)	0.30	0.05	0.05	Variable	0.01
Band gap Eg (in eV)	3.3	3.3	2.7	1.1	1.10
Electron affinity (in eV)	4.40	4.40	4.02	4.20 10.00	4.14
Dielectric permittivity (εr)	9.00	9.00	10.00	2.2E+18	13.60
CB effective density of states (cm^{-3})	1.0E+18	1.0E+18	1.0E+18	1.8E+19	2.2E+18
VB effective density of states (cm^{-3})	1.0E+19	1.0E+19	1.0E+19	1.0E+7	1.8E+19
Electron-thermal velocity (cm/s)	1.0E+7	1.0E+7	1.0E+7	1.0E+7	1.0E+7
Hole-thermal velocity (cm/s)	1.0E+7	1.0E+7	1.0E+7	1.0E+2	1.0E+7
Electron mobility (cm^2/vs)	1.0E+2	1.0E+2	5.0E+1	2.5E+1	1.0E+2
Hole mobility (cm^2/vs)	2.5E+1	2.5E+1	2.0E+1	0	2.5E+1
Donor density ND (cm^{-3})	1.0E+18	1.0E+17	1.0E+17	1.0E+15	000
Acceptor density NA (cm^{-3})	0	1.0E+17	0.0E0		1.0E15

- Electronic absorption

The absorption coefficient vslue for CZTSe ($Cu_2ZnSnSe_4$) is a key optical property that highlights its efficiency as a solar-cell absorber layer. This material exhibits a very high absorption coefficient, typically exceeding 10^4 to 10^5 cm^{-1}, in visible and near-infrared (NIR) spectral ranges. This confirms the ability of the material to effectively absorb light even at small thicknesses. The absorption curve, Fig. 4, shows relatively high absorption coefficient values at bandgap energies ranging 1.0–1.1 eV [3–5]. Together with the higher coefficient values at shorter wavelengths, the material is able to capture a broad portion in the solar spectrum. This implies that CZTSe can convert a significant amount of solar energy into electricity, making it a strong candidate as a sustainable alternative in thin-film solar technologies. Moreover, the high absorption coefficient allows for using smaller layer thicknesses without compromising light absorption efficiency.

Typically, material structures affect their optoelectronic properties [59]. Varying crystal structure affects a material band gap, conductivity and properties. Order and deffects also affect materials optoelectronic properties [60].

Like other materials, the CZTSe optical properties and performance, in solar cells, depend primarily on both the crystal structure, order and the elemental composition. The ordered kesterite phase provides a suitable band gap with strong light absorption, while structural disorder, particularly Cu/Zn site exchange, introduces deep defect states [61]. This increases recombination and lowers the V_{OC}. From a compositional standpoint, the Cu-poor/Zn-rich regime is considered optimal, as it minimizes structural defects and suppresses harmful secondary phases. This improves carrier lifetime and performance. In contrast, Cu-rich or Sn-rich conditions favor the formation of conductive or insulating secondary phases that hinder charge transport [62]. Selenium content is also highly critical, since Se deficiency leads to vacancies that act as recombination centers [63]. Therefore, combining an ordered crystal structure with a Cu-poor/Zn-rich composition and sufficient Se saturation is the key to improve the optoelectronic properties and enhance the overall efficiency.

- Contact angle

The contact angle, which is the angle between a solid surface and a tangent of liquid droplet, being water here, at the point of contact with the air. It is used as an indicator to assess surface properties, especially wettability. A contact angle $<90^\circ$ indicates that the surface is hydrophilic, meaning the liquid tries to spread all over the surface. A contact angle $>90^\circ$ means the surface is hydrophobic, where the liquid prefers to form droplets and does not spread easily [64]. The contact angle is affected by various factors, including surface energy, roughness, and the presence of active chemical groups.

In Fig. 5, the contact angle for the absorber layer is less than 90 degrees, indicating that the surface exhibits hydrophilic behavior. This is desirable in many applications, particularly in solar cells and opto-electronic devices, for more than one reason. Firstly, this yield improved wetting of subsequent layers. A lower contact angle means that

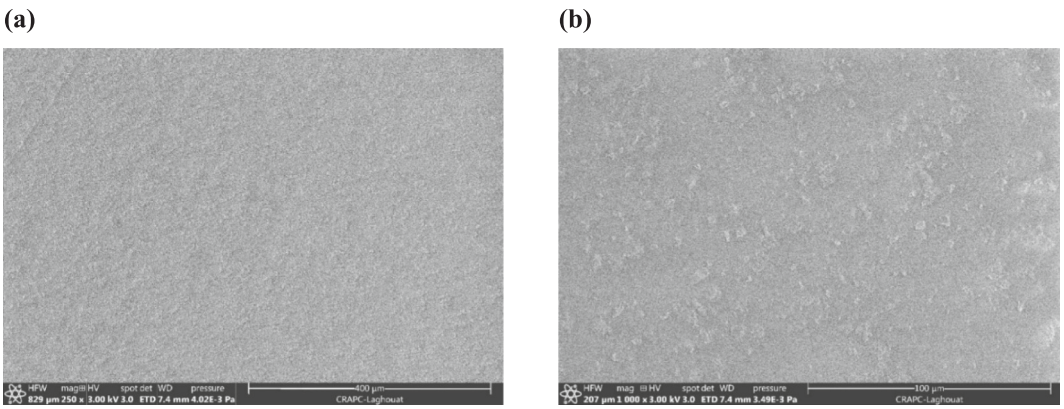

Fig. 2. SEM images measured for the CZTSe thin film surface at two different magnifications.

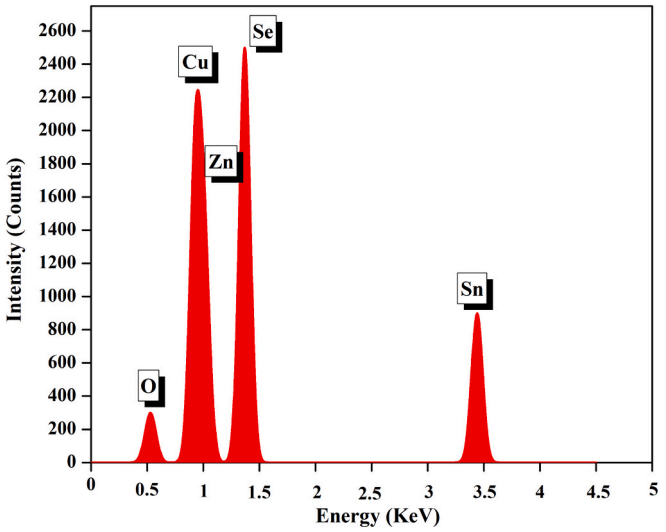

Fig. 3. EDAX spectrum measured for the CZTSe film.

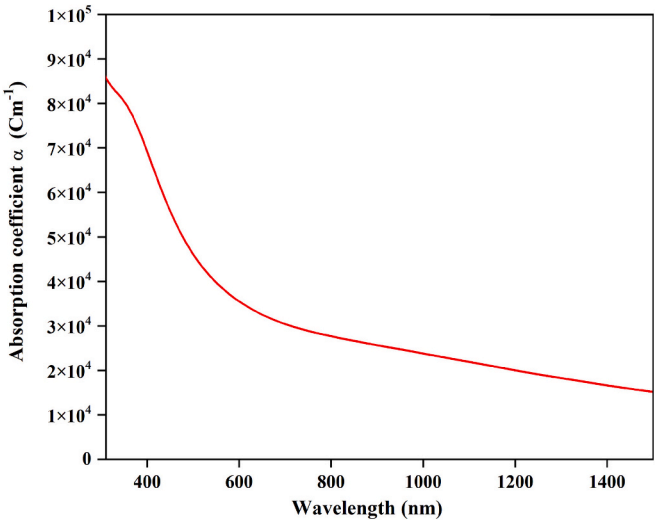

Fig. 4. Values of absorption coefficient measured for CZTSe vs. wavelength.

Table 2
CZTSe film elemental composition measured from EDAX analysis.

Element	Atomic %	Weight %	Notes
Cu	22.5	19.3	Slightly high
Zn	12.8	9.7	Zn-rich
Sn	10.5	18.2	Balanced
Se	52.0	47.5	Slight excess
O	2.2	5.3	Likely from surface oxidation or air

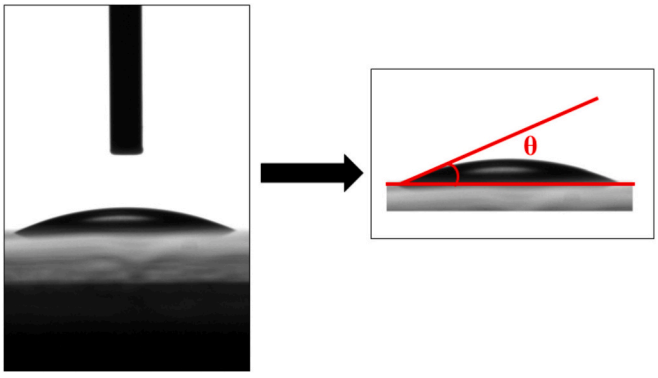

Fig. 5. Water contact angle on the CZTSe film surface.

subsequent layers, such as conductive or transparent films, will spread more uniformly and form better adhesion with the absorber layer. Secondly, the surface exhibits good interfacial adhesion. This enhances structural uniformity, lowers interfacial defects and positively affects the device photoelectric performance. Thirdly, optical properties are improved. Hydrophilic behavior, especially when combined with slight surface roughness, can improve light absorption by lowering reflection and increasing the optical path within the material. Therefore, the measured contact angle values here support the suitability of the absorber layer in terms of surface characteristics for light absorption and solar energy applications [65].

- Surface profiling

To further investigate the surface, its roughness has been investigated using surface profilometry, Fig. 6. Ra and Rz are among the most important parameters in surface roughness analysis or surface profiling. Ra represents the arithmetic average of the surface height deviations from the mean line and provides an overall indication of how smooth or rough the surface is lower Ra values indicate a smoother surface. On the other hand, Rz refers to the average difference between the heights of the highest five peaks and the depths of the deepest five valleys within the measured length, making it a sensitive indicator of sharp defects and surface irregularities. Therefore, Ra reflects the general roughness, while Rz reveals significant variations in height, and both are essential

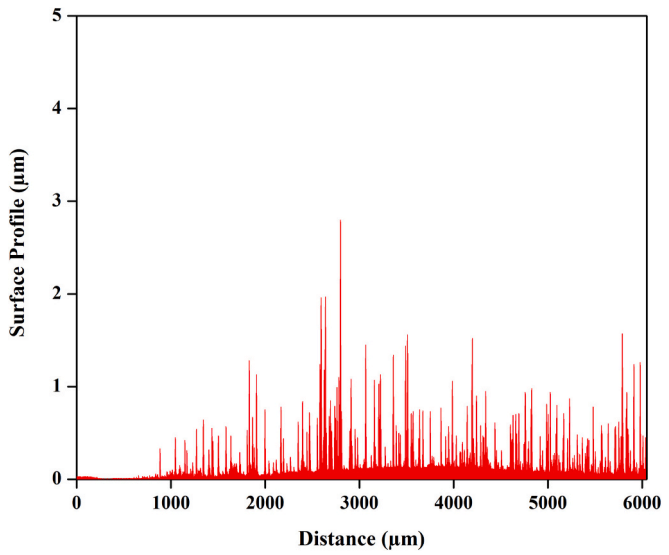

Fig. 6. Topographical line scan measured for the CZTSe film surface.

for evaluating surface quality in precision applications.

Ra and Rz values are summarized in Table 3. The average value for Ra is 0.14 µm. This is a good to moderate value. The surface is not very smooth like those of ultra-thin film layers with less than 0.02 µm, but it is suitable for absorber layers, as roughness may improve light absorption and lowers reflection, depending on incident photons [66],[67]. The Rz value is 3.04 µm, which is normal and acceptable for layers that require texturing to enhance light absorption. The area (1224.7 μm^2) is considered reasonable for reliable analysis. It is neither too small nor too large, and it provides representative results of the surface quality in that region.

The values are suitable for fabricated absorber layers in solar energy applications. Roughness at this level may improve photon absorption by decreasing reflection and increasing the optical path within the material. The micro-scale peaks and valleys enhance photon absorptions within the active layers, thereby increasing charge generation. The balanced rough surface also improves contact between the CZTSe layer and adjacent layers, by improving adhesion [27],[68]. This facilitates the transport of holes and electrons to the electrodes, lowers interface recombination rate and series resistance. It also improves V_{OC} and FF. Thus, the surface roughness improves both photon absorption and charge transport, contributing directly to the solar cell performance.

3.2. Simulation results

In above sections, the CZTSe layer suitability for the proposed solar cell is confirmed based on experimentally measuring its physical properties. The suitability of the CZTSe is now assessed by studying its photovoltaic characteristics in the proposed solar cell metal/$MoSe_2$/CZTSe/ZnSe/i-ZnO/ZnO-Al/metal. Two main features for the CZTSe layer, namely its doping concentration and thickness, are optimized here to exhibit the solar cell potentials, in comparison with earlier literature systems.

Table 3
CZTSe film surface parameters Ra and Rz. Measurements are made over an area of 1224.7 μm^2.

	Ideal	In this work
Ra	0.05 to 0.3 µm	0.14 µm
Rz	1 to 5 µm	3.04 µm

- Effect of CZTSe layer thickness

Literature showed that the CZTSe absorber-layer thickness critically affects affects solar cell power conversion efficiency (*PCE*) due to its direct influence on both light absorption and carrier collection efficiency [17]. In very thin layers, absorption is insufficient, particularly at longer wavelengths, which leads to a lower J_{SC} and consequently to a lower PCE. However, further increasing the thickness typically introduces adverse effects, such as enhanced bulk recombination due to higher structural and chemical defect density, reduced transport efficiency of carriers generated deep within the absorber, and an increase in R_S. These combined effects contribute to a decrease in the overall efficiency [17]. For these reasons, effect of CZTSe absorber layer thickness on all cell parameters *Jsc*, V_{OC}, *FF)* and *PCE* has been studied.

Effect of CZTSe layer thickness on solar-cell performance is investigated here, while other parameters are being kept unchanged, Table 1. The absorber thickness is varied in a wide range of 0.5 to 4.0 µm. The results are exhibited in Fig. 7. Fig. 7a describes how *J-V* plots are affected by CZTSe layer thickness. In Fig. 7b, the quantum efficiency (*QE*) values, calculated in the range 400–1230 nm, clearly vary with the layer thickness, with optimal thickness being 2.5 µm.

As shown in Fig. 7, larger CZTSe layer thickness improves *Jsc* from 46.521 to 48.513 mA/cm^2. This improvement is primarily due to increased photon absorption with thicker layers, yielding a higher generation rate of electron & hole pairs. This resembles literature results where absorption increases with thickness [69],[70]. Additionally, a thicker layer for the absorber lowers the charge-carrier recombination probability. The extended volume provides carriers with a greater opportunity to diffuse and reach the contacts before recombining, thereby further enhancing *Voc*. However, high thicknesses cause higher recombination, which in turn lowers the J_{SC} value [71]. This is understandable in the present study, Fig. 7(c). The J_{SC} value increases with increasing thickness at first, reaching a maximum value at the optimal thickness 2.5 µm, before decreasing.

Effect of CZTSe film thickness on *FF* is described in Fig. 7(c). *FF* increases with increasing thickness until a maximum value of 77 % is reached at 2.5 µm. The result is understandable as higher thickness yields higher photon absorption that yields more electron hole-pairs. That After the optimal thickness values, *FF* decreases with increased thickness. That is because higher thicknesses encourage recombination processes (SRH, Auger, or radiative). With higher thickness, carriers have longer transit distances with higher probability to get trapped in defects, which increases recombination and decreases cell performance.

Larger CZTSe layer thickness increases the *Voc* reaching a maximum value 0.478 V at 2.5 µm, Fig. 7c. This is in congruence with other earlier literature. With higher thickness, recombination is lowered. More electrons exist and a higher electrical field occurs yielding higher V_{OC}. These behaviors profoundly occur at the optimal thickness. However, this positive effect on *Voc* is most evident when the material has relatively low defect density and sufficient carrier diffusion length [72]. After the optimal thickness, the V_{OC} decreases. This is expected as too high thickness increases the diffusion distance and allows more recombination and loss of charges in the space-charge layer. Thus, the electrical field build up is lowered at the interfaces and V_{OC} is lowered.

With increased *Jsc*, *FF* and *Voc* values, the overall power conversion efficiency (η) assumes a high value of 17.92 %, at the optimal thickness, Fig. 7(c). At higher thicknesses, more trap states occur yielding higher recombination and lower efficiency. This is natural as efficiency is related to all characteristics, Eq. (4).

$$\eta = \frac{V_{oc} \times J_{sc} \times FF}{P_{in}} \tag{4}$$

where η efficiency and *Pin* incident-light power density (usually 100 mW/cm^2 at AM 1.5G illumination).

All-in-all, the optimal thickness 2.5 µm is the one that ensures highest

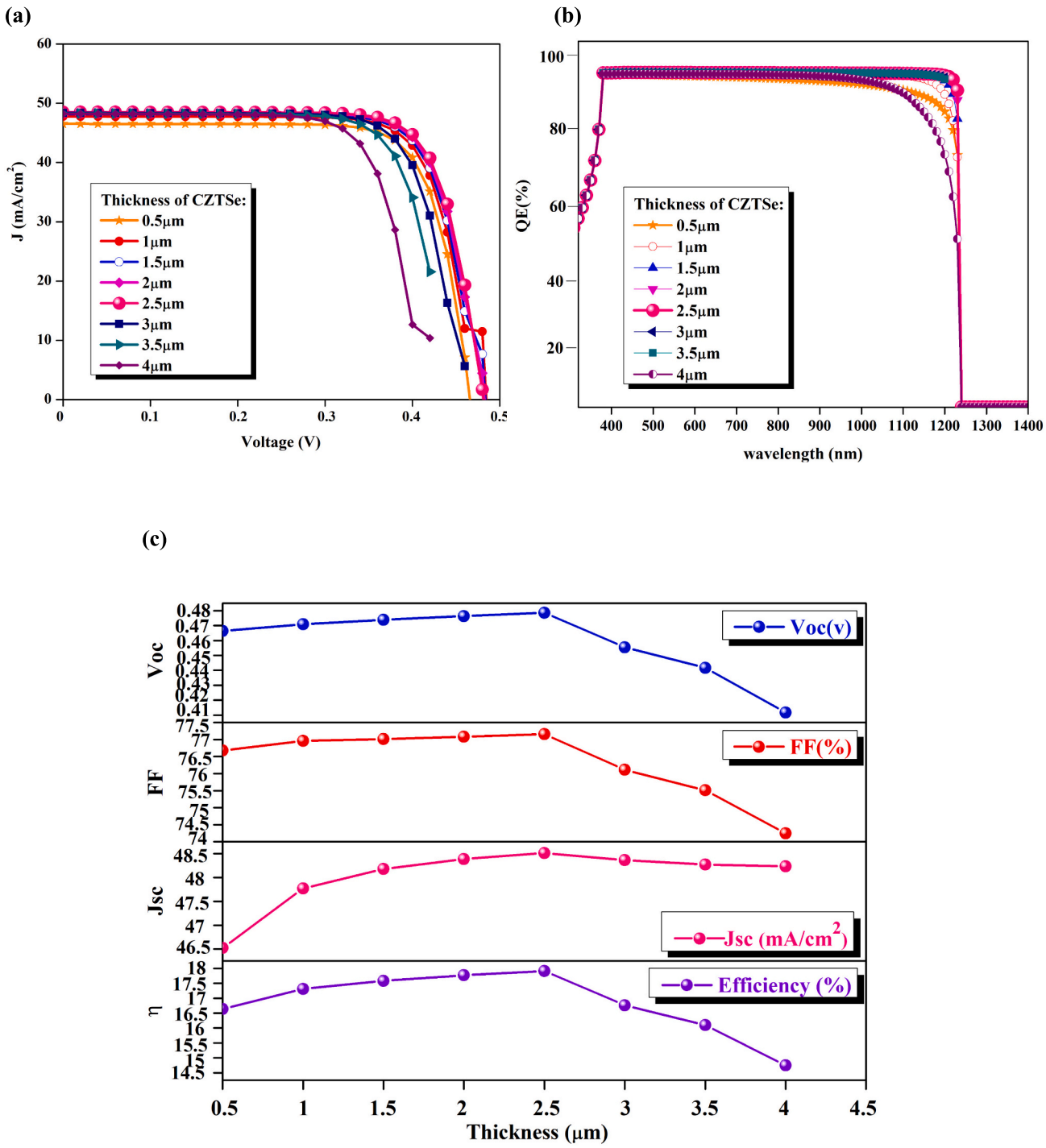

Fig. 7. CZTSe-layer thickness effect on proposed solar-cell characteristics. (a) *J-V* plots, (b) Quantum efficiency (*QE)* variation with wavelength (c) *FF* (%), J_{SC} (mA/cm^2), *Voc* (V) and η (%).

possible light absorption, optimal travel distance, lowest resistance and lowest recombination in the proposed solar cell. Naturally, higher η is achieved.

- Effect of CZTSe layer doping concentration

Considering the optimal value for CZTSe layer thickness is 2.5 µm, the layer doping concentration is varied between 1×10^{15} and 5×10^{19} cm^{-3}. Effects of varying CZTSe layer-doping concentration on the solar cell characteristics are exhibited in Fig. 8.

Fig. 8(a) presents *J–V* plots which vary with doping concentration. From Fig. 8 (b), the quantum efficiency (*QE*), calculated in the range 400–1230 nm, slowly increases with CZTSe doping concentration from 1×10^{15} to 5×10^{16} cm^{-3}. At higher than the optimal concentration 5×10^{16}, the *QE* decreases sharply. The *QE* change with doping concentration resembles that in η change, vide infra.

In Fig. 8(c), the cell characteristics vary with doping concentration. At lower doping concentrations, J_{SC} only slightly increases to ~47 mA/cm^2 value with increased concentration. The slow increase is a balance off between increased conductivity and crystallite disorder that increases recombination, by increased concentration. At doping concentrations higher than 5×10^{16} cm^{-3}, the J_{SC} decreases readily. Similar

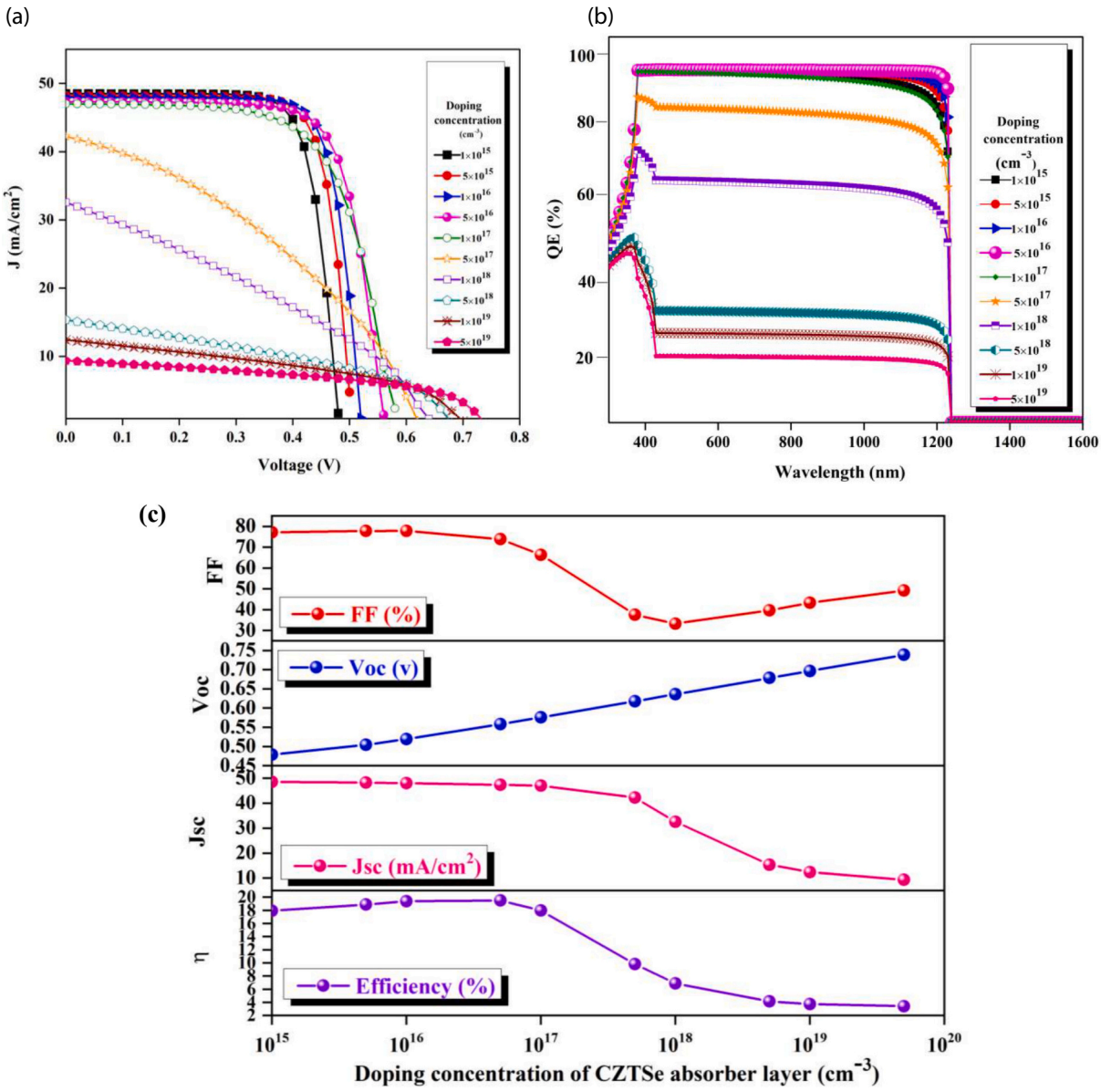

Fig. 8. Effect of CZTSe-layer doping concentration on solar-cell characteristics. (a) *J-V* plots, (b) *QE* variation with wavelength (c) *FF* (%), J_{SC} (mA/cm^2), V_{OC} (v) and η (%).

behaviors were observed in other systems, where J_{SC} increased with doping concentration to a limit after which the J_{SC} decreased [73],[74]. It should also be noted that the relation between doping concentration and J_{SC} value is not simple and widely varies between various types of solar cell materials [75]. Overall, the J_{SC} current increase with higher doping concentration is due to improved conductivity and lowered serial resistance. Much higher doping concentrations affect the crystallite quality and increase its disorders, which increases traps in the crystallites. This will impede current, and increase recombination processes, yielding lower J_{SC} values. Therefore, maximum J_{SC} values are expected to occur at optimal doping density, as observed here.

A similar behavior is observed in *FF* that assumes nearly constant value of 73.8 %. At doping concentrations higher than 5×10^{16} cm^{-3}, *FF* decreases. Similar behaviors are known in various semiconducting material solar cells where optimal doping concentrations are determined [75],[76]. As the doping concentration increases conductivity increases, but this is possibly counteracted by increased crystallite disorder and recombination. At much higher concentrations, the crystallites become highly disordered which increases recombination. In the present study, the optimal doping concentration for highest *FF* is 5×10^{16} cm^{-3}.

From Fig. 8(c), V_{OC} slowly increases with doping concentration increase at the beginning. The tendency then continues to increase nearly linearly, albeit at only a small rate, with increased doping concentration. In earlier literature, conflicting trends for doping concentration effects on V_{OC} were reported. In some reports, V_{OC} value increased with doping concentrations, presumably due to depletion layer narrowing and carrier recombination lowering at the p-n junction [77]. Other studies showed that V_{OC} increased with higher doping up to a limit after which the value decreased [78]. In other cases, V_{OC} decreased with increased concentration [79]. V_{OC} also exhibited little changes by varying doping concentration in other reports [80]. Typically, higher concentration allows higher electrical field build up at the interfaces which increases V_{OC}. At much higher concentrations, recombination increases due to more trap formation which lowers cell efficiency. As per V_{OC} here, it continues to increase with higher doping concentrations when working within the current concentration values.

As per η, it is affected by V_{OC}, *FF* and J_{SC} together, as summarized in Eq. (4). Therefore, the η varies with doping concentration depending on

how these three characteristics vary, as a balance off. Fig. 7(c) indicates that η increases slowly to a 19.5 %-maximum value at the optimal concentration 5 × 10^{16} cm^{-3}, after which the efficiency decreases quickly.

- Current and charge-density distribution in the solar cell

Having determined the optimal thickness and doping concentrations for CZTSe absorber layer at 2.5 μm and 5 × 10^{16} cm^{-3}, respectively, charge carriers -electrons and holes- behaviors within the multi-layer solar cell structure are analyzed. The cell involves $MoSe_2$ as a back contact, CZTSe as an absorber layer and ZnSe as a window layer and a front contact. Fig. 9 presents simulation results showing the current and charge density distributions within the cell. This helps in understanding the mechanisms of charge separation and transport, together with effects of various layers on the photovoltaic cell performance. Fig. 9(a) presents the distribution of current density for electrons (*Jn*) and holes (*Jp*) across the layered structure of a solar cell involving $MoSe_2$/CZTSe/ZnSe. The current densities are shown on the vertical axis (in mA/cm^2) against the spatial position (μm) on the horizontal axis, extending from $MoSe_2$ back contact to ZnSe front contact. The electron current density (*Jn*) is positive in the ZnSe layer and gradually decreases across the CZTSe layer, becoming negative at the $MoSe_2$ side. On the other side, the hole current density (*Jp*) follows the opposite behavior. This indicates that most electrons are moving toward the front contact (ZnSe), while holes move toward the back contact ($MoSe_2$), as expected in p-n type solar cells [81]. Charge carrier motions are driven by internal electrical fields.

The sharp change in current near the interfaces, especially at the CZTSe/ZnSe interface, suggests a strong compositional or electric field gradient at that point, contributing to efficient charge separation. The nearly flat behavior in the middle of the CZTSe layer indicates a neutral region where chare generation and recombination are approximately balanced, showing that CZTSe functions effectively as an absorber layer. The largely symmetrical distribution between *Jn* and *Jp* reflects effictive charge separation and transportation within the solar cell, which is a positive indicator of current collection, power generation and consequently cell performance.

Fig. 9(b) shows the distribution of carrier densities (electrons in blue, holes in red) across the solar cell structure ZnO:Al/i-ZnO/ZnSe/CZTSe/$MoSe_2$, revealing a clear gradient that reflects the properties of each layer. Electron concentration is high on the right side (ZnO:Al – n-type) and gradually decreases upon entering the CZTSe layer (p-type). The hole concentration behaves oppositely, being high in the CZTSe absorber and decreasing near the ZnSe and $MoSe_2$ interfaces. The Figure clearly indicates the n- and p-type regions. Sharp changes in carrier concentrations at the layer interfaces, especially between ZnSe/CZTSe and CZTSe/$MoSe_2$, points to depletion regions. The depletion regions are responsible for charge separation. This drives electrons toward ZnO front contact and holes toward Mo back contact, ensuring efficient solar cell operation.

- Solar-cell band diagram structure

To better understand physical phenomena inside the cell, energy-band diagram for CZTSe-based solar cell has been studied, Fig. 10. With a band gap value ~1.0 eV, CZTSe acts as the main absorber layer, where photons are being absorbed and consequently electron-hole pairs are being generated. On the left side, there is a band bending at the CZTSe/Mo interface, indicating the presence of an intermediate $MoSe_2$ layer. This is essential for enhancing hole collection and lowering

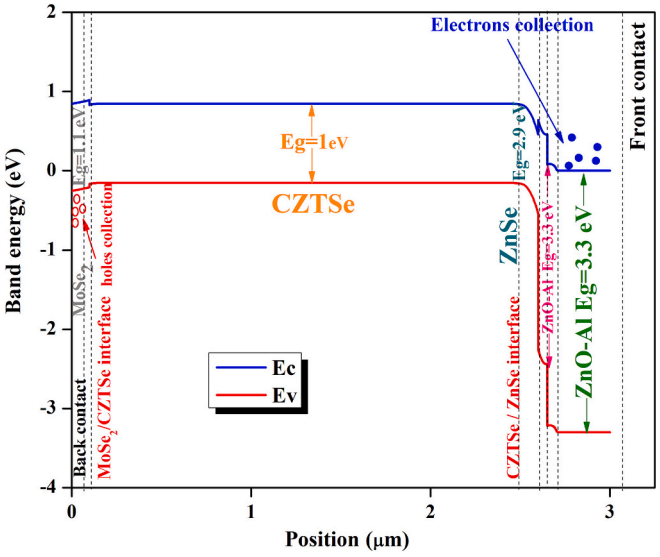

Fig. 10. The band diagram for the proposed CZTSe-based solar cell.

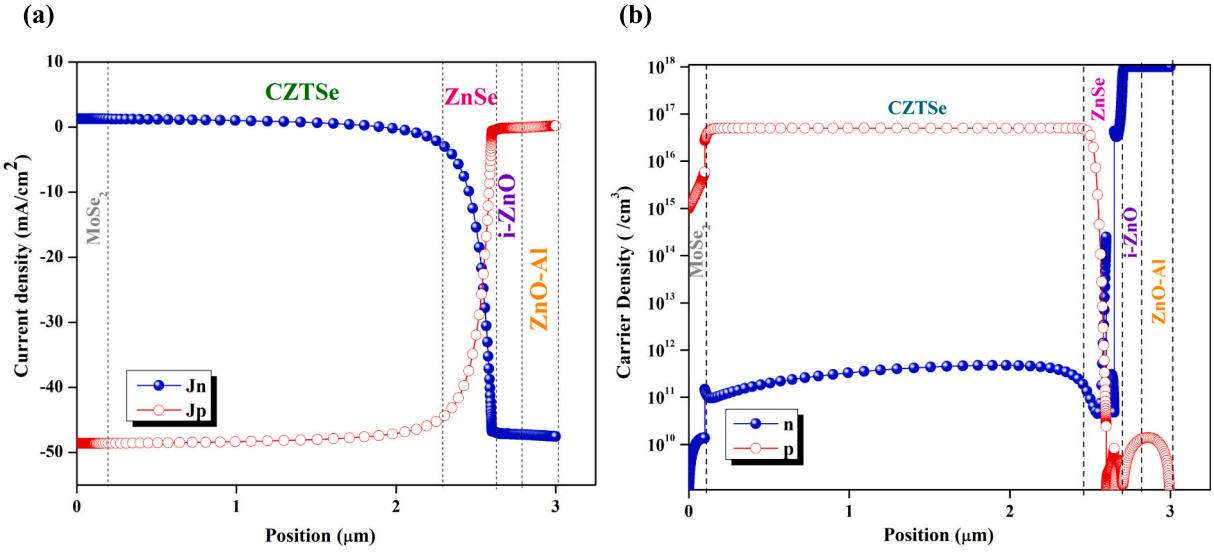

Fig. 9. Distribution of current and carrier densities vs. distance across simulated solar cell layers. (a) Current density and (b) Charge density. Blue refers to electrons, red refers to holes.

surface recombination. On the right side, distinct energy band transitions are observed from CZTSe to ZnS and then to ZnO:Al. This suggests the formation of energy barriers that facilitate charge separation and electron transport toward the front contact. ZnS serves as a buffer layer, with a wider energy-band gap ($Eg \approx 3.0$ eV) to prevent surface recombination of electrons. ZnO:Al functions as a transparent conductive oxide (TCO) allowing efficient electron transport to the front contact. This energy alignment between layers enhances charge separation and improves the overall cell efficiency. Moreover, electron collection occurs at the ZnO:Al/ZnS interface, indicating well-optimized energy levels to minimize energy losses due to recombination.

All in all, the optimal proposed solar cell involves a CZTSe layer thickness 2.5 μm and a doping concentration 5×10^{16} cm^{-3}. The optimal proposed cell exhibits the *J-V* quantum efficiency plots described in Fig. 11(a) and (b), respectively. The solar cell characteristics are presented in Table 4.

Results indicate that the present solar cell is superior to earlier CZTSe-based systems in more than one aspect, as summarized in the comparison Table 4. Firstly, the present solar cell exhibits higher performance than earlier ones, entries 1–7. Secondly, the present solar cell needs no hazardous materials such as Cd by comparing entries 1 with entries 3, 6 and 7. Thirdly, the proposed cell does not involve costly elements such as Ag or Ge, by comparing entry 1 with entries 2–4. Therefore, all goals and assumptions stated in Section 1 above are achieved here.

Despite these features, the present study if not free of limitations. The proposed solar cell stability has not been investigated here. Literature showed that CZTSe based solar cells may not be specially stable. The CZTSe/CdS junctions are known to be specially unstable [82], but fortunately the CdS has been avoided here. CZTSe material is also known to be unstable to heat, air and moisture. For this reason, attempts were made to stabilize the layer by doping with the costly Ge [83]. Using fluorine-doped tin oxide (FTO) as substrates instead of tin-doped indium oxide (ITO) or molybdenum (Mo) were also reported to stabilize CZTSe/CdS based solar cells [82]. Therefore, attempting the abundant FTO/glass substrates is strongly recommended for the present solar cell. Annealing the CZTSe layer at 400 °C was also reported to stabilize solar cells [63]. Fortunately, the CZTSe layer has been annealed here at 500 °C with no observed changes on its properties. The CZTSe layer stoichiometry affects the CSTZe solar cell stability [84]. In the present study, EDX results indicated a suitable stoichiometry for the CZTSe, as described above.

The present cell has not been physically prepared or experimentally examined for stability. This is another issue to be considered. Studying impact of photovoltaic usage of the proposed cell, involving ZnSe as a replacement for CdS, and on its physical properties has not been achieved. It is strongly recommended to undertake such a study both experimentally and theoretically by DFT for example. More study needs to be made on the passivating effect of the ETL buffer layer, since buffer layers normally exhibit passivation and stabilization on the absorber layers in various solar cell [85],[86]. Future studies should also include effects of defect densities of various layers.

Table 4
Optimized CZTSe-based solar cell characteristics compared with relevant literature.

Entry #	Cell description	*Voc* (V)	*Jsc* (mA/cm^2)	*FF* (%)	*η* (%)	Ref.
1	ZnO:Al/i-ZnO/ZnSe/CZTSe/$MoSe_2$	0.56	47.33	73.82	19.50	This work
2	CZTSe electrodeposited with Ge doping	0.73	21.74	69.27	10.54	[23]
3	CdS(n)/$(Ag_xCu_{1x})_2ZnSnSe_4$(p)/$Cu_2ZnSnSe_4$(p +)	0.42	35.84	65.20	9.81	[35]
4	Ge-doped CZTSe solar cells.	0.47	37.9	82.5	14.00	[37]
5	Ag-Ge doped CZTSe thin films	0.423	36.8	65.7	10.23	[36]
6	ZnO/CdS/CZTSe/$MoSe_2$/Mo	0.35	30	60	6.50	[89]
7	CdS/CZTSe/$MoSe_2$	0.42	35.8	66	9.50	[34]

4. Conclusion

In an effort to maximize CZTSe-based solar cells, while minimizing their environmental impact and lowering their cost, a new solar cell structure is presented here. The structure is summarized as metal/$MoSe_2$/CZTSe/ZnSe/i-ZnO/ZnO-Al/metal. The hazardous CdS buffer layer is replaced here with a safe ZnSe layer. Doping with costly elements, such as Ag or Ge is avoided. The CZTSe absorber layer is experimentally prepared by the simple sol-gel technique and characterized by ATIR spectra, electronic absorption spectra, SEM, EDX, profilometry and contact angle measurement. The material characteristics confirm its suitability for absorber in solar cells, as a homogeneous surface with the proper stoichiometry. Furthermore, the solar cell has been simulated, focusing on effects of thickness and doping concentration, of the CZTSe-absorber layer, on the device performance. Simulation results indicate highest solar cell characteristics of open circuit

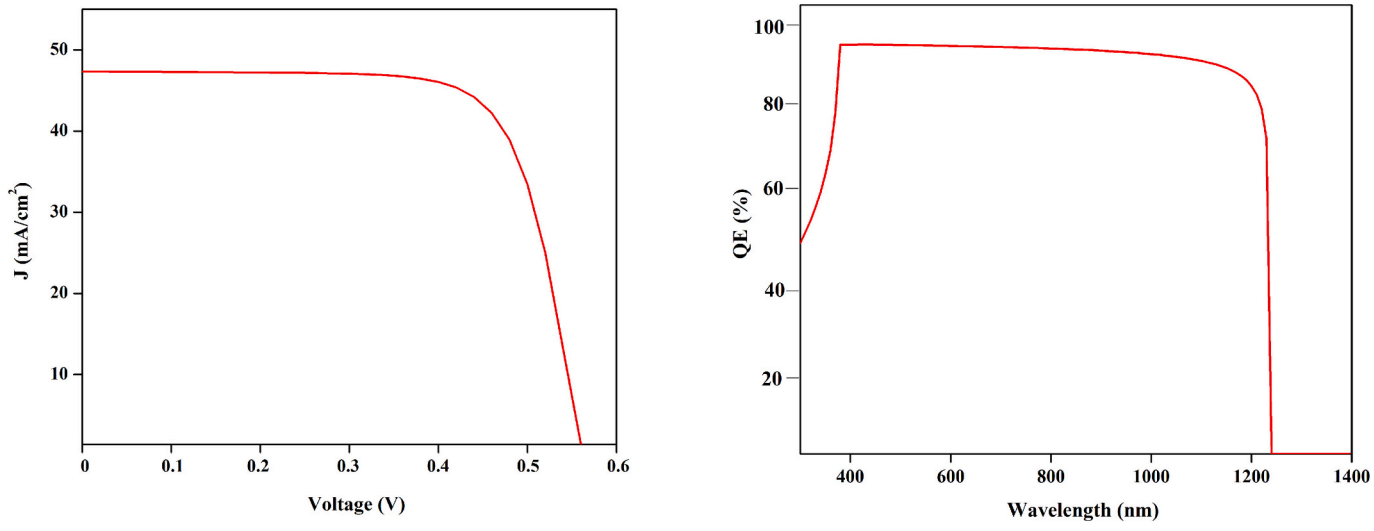

Fig. 11. The simulated *J-V* and *QE* plots for the optimized solar cell.

potential 0.56 V, short circuit photocurrent density 47.33 mA/cm^2 and fill factor 73.82 %. A new high overall conversion efficiency value of 19.50 % is achievable at the optimal absorber layer thickness of 2.5 μm and a doping level of 5 × 10^{16} cm^{-3}. These findings confirm the potential of sol-gel synthesized CZTSe as an effective and viable material for a high-performance thin-film solar cell. The proposed solar cell is superior to earlier similar cells in terms of performance, eco-friendliness and material costs.

CRediT authorship contribution statement

Feriha Afrah Boukhelkhal: Writing – original draft, Software, Investigation. **Naceur Selmane:** Writing – review & editing, Supervision, Methodology. **Ali Cheknane:** Supervision, Project administration, Funding acquisition. **Moustafa Noureddine:** Conceptualization. **Abdelhalim Zoukel:** Investigation. **Nilgun Baydogan:** Investigation. **Büşra Günalan:** Investigation. **Hikmat S. Hilal:** Validation, Writing – review & editing.

Declaration of competing interest

The authors declare that they have no known competing financial interests or personal relationships that could have appeared to influence the work reported in this paper.

Acknowledgment

N.S. & A.C. acknowledge Amar Telidji University-Laghouat financial support, through the PRFU Project # A10N01UN030120220002: “Contribution à l’étude des propriétés physico-chimiques des nouveaux matériaux: Applications dans le domaine des énergies renouvelables”. They also thank “La Direction Générale de la Recherche Scientifique et du Développement Technologique (DGRSDT)”.

Data availability

All data are shown in the manuscript, and additional data will be provided upon request.

References

[1] S. Chen, X.G. Gong, A. Walsh, S.-H. Wei, Crystal and electronic band structure of Cu2ZnSnX4 (X=S and Se) photovoltaic absorbers: first-principles insights, Appl. Phys. Lett. 94 (2009) 041903, https://doi.org/10.1063/1.3074499.
[2] A. El Khalfi, K. Ridani, L. Et-taya, A. El Boukili, N. Mansour, L. Elmaimouni, Md. F. Rahman, A. Benami, Dual-absorber solar cell design and simulation based on Sb2Se3 and CZTGSe for high-efficiency solar cells, Langmuir 40 (2024) 20352–20367, https://doi.org/10.1021/acs.langmuir.4c01472.
[3] A. Kumar, Theoretical analysis of CZTS/CZTSSe tandem solar cell, Opt. Quant. Electron. 53 (2021) 528, https://doi.org/10.1007/s11082-021-03183-5.
[4] T. Chargui, F. Lmai, K. Rahmani, Improving the performance of a tandem cell based on Sb2S3/CZTSe: numerical study, J. Opt. (2024), https://doi.org/10.1007/s12596-024-02117-0.
[5] D.B. Khadka, J. Kim, Band gap engineering of alloyed Cu_2 ZnGe $_x$ Sn $_{1-x}$ Q_4 (Q = S, Se) films for solar cell, J. Phys. Chem. C 119 (2015) 1706–1713, https://doi.org/10.1021/jp510877g.
[6] V. Kumar, U.P. Singh, Effect of selenization temperature on the formation of CZTSe absorber layer, Appl. Phys. A Mater. Sci. Process. 125 (2019) 808, https://doi.org/10.1007/s00339-019-3113-8.
[7] K.J. Tiwari, R. Chetty, R.C. Mallik, P. Malar, Solid state synthesis and e-beam evaporation growth of Cu2ZnSnSe4 for solar energy absorber applications, Sol. Energy 153 (2017) 173–180.
[8] H. Arbouz, Modeling of a tandem solar cell structure based on CZTS and CZTSe absorber materials, Int. J. Comp. Exp. Sci. Eng. 8 (2022) 14–18.
[9] L. Sravani, S. Routray, M. Courel, K.P. Pradhan, Loss mechanisms in CZTS and CZTSe Kesterite thin-film solar cells: understanding the complexity of defect density, Sol. Energy 227 (2021) 56–66.
[10] M.S. Rana, M.M. Islam, M. Julkarnain, Enhancement in efficiency of CZTS solar cell by using CZTSe BSF layer, Sol. Energy 226 (2021) 272–287.
[11] L. Et-taya, A. El Khalfi, M. Hamdaoui, A. El Boukili, L. ELMaimouni, N. Mansour, M.F. Rahman, A. Benami, High-efficiency CZTSSe/CIGSe ultra-thin structures for next-generation solar cells with 45.40% efficiency, J. Opt. (2025), https://doi.org/10.1007/s12596-025-02781-w.
[12] B. Islam, T.M. Khan, Md.F. Rahman, S.R.A. Ahmed, Efficiency enhancement of copper indium gallium Diselenide-based thin-film solar cell with copper iodide as hole-transport layer: a simulation approach, Phys. Status Solidi A 222 (2025) 2400776, https://doi.org/10.1002/pssa.202400776.
[13] N. Selmane, A. Cheknane, F. Khemloul, M.H.S. Helal, H.S. Hilal, Cost-saving and performance-enhancement of CuInGaSe solar cells by adding CuZnSnSe as a second absorber, Sol. Energy 234 (2022) 64–80, https://doi.org/10.1016/j.solener.2022.01.072.
[14] K.T. Arockiadoss, A.-D. Rasu Chettiar, M.F. Rahman, M.K. Hossain, L. Marasamy, Architecture guidelines for Cu2SrSnS4 solar cells using chalcogenide and oxide hole transport layers by SCAPS-1D simulation, J. Phys. Chem. Solids 203 (2025) 112732, https://doi.org/10.1016/j.jpcs.2025.112732.
[15] Y.-F. Du, J.-Q. Fan, W.-H. Zhou, Z.-J. Zhou, J. Jiao, S.-X. Wu, One-step synthesis of stoichiometric Cu_2 $ZnSnSe_4$ as counter electrode for dye-sensitized solar cells, ACS Appl. Mater. Interfaces 4 (2012) 1796–1802, https://doi.org/10.1021/am3000616.
[16] I.L. Repins, M.J. Romero, J.V. Li, S.-H. Wei, D. Kuciauskas, C.-S. Jiang, C. Beall, C. DeHart, J. Mann, W.-C. Hsu, Kesterite successes, ongoing work, and challenges: a perspective from vacuum deposition, IEEE J. Photovolt. 3 (2012) 439–445.
[17] A. Bag, R. Radhakrishnan, R. Nekovei, R. Jeyakumar, Effect of absorber layer, hole transport layer thicknesses, and its doping density on the performance of perovskite solar cells by device simulation, Sol. Energy 196 (2020) 177–182, https://doi.org/10.1016/j.solener.2019.12.014.
[18] U. Syafiq, E. Isotta, N. Ataollahi, K. Lohani, S. Luong, V. Trifiletti, O. Fenwick, P. Scardi, Facile and low-cost fabrication of Cu/Zn/Sn-based ternary and quaternary chalcogenides thermoelectric generators, ACS Appl Energy Mater 5 (2022) 5909–5918, https://doi.org/10.1021/acsaem.2c00268.
[19] L. Yao, J. Ao, M.-J. Jeng, J. Bi, S. Gao, Q. He, Z. Zhou, G. Sun, Y. Sun, L.-B. Chang, J.-W. Chen, CZTSe solar cells prepared by electrodeposition of Cu/Sn/Zn stack layer followed by selenization at low se pressure, Nanoscale Res. Lett. 9 (2014) 678, https://doi.org/10.1186/1556-276X-9-678.
[20] Y. Zhao, C. Xu, N. Yu, Z. Zhou, Y. Chen, X. Hu, Y. Zhang, S. Wang, A DMSO/MOE mixed solvent system for improving the morphology and efficiency of kesterite solar cell, Sol. Energy 258 (2023) 294–303.
[21] A. Redinger, D.M. Berg, P.J. Dale, S. Siebentritt, The consequences of Kesterite equilibria for efficient solar cells, J. Am. Chem. Soc. 133 (2011) 3320–3323, https://doi.org/10.1021/ja111713g.
[22] A. Chirilă, P. Reinhard, F. Pianezzi, P. Bloesch, A.R. Uhl, C. Fella, L. Kranz, D. Keller, C. Gretener, H. Hagendorfer, Potassium-induced surface modification of Cu (In, Ga) Se2 thin films for high-efficiency solar cells, Nat. Mater. 12 (2013) 1107–1111.
[23] C. Yan, J. Huang, K. Sun, S. Johnston, Y. Zhang, H. Sun, A. Pu, M. He, F. Liu, K. Eder, Cu2ZnSnS4 solar cells with over 10% power conversion efficiency enabled by heterojunction heat treatment, Nat. Energy 3 (2018) 764–772.
[24] W. Wang, M.T. Winkler, O. Gunawan, T. Gokmen, T.K. Todorov, Y. Zhu, D.B. Mitzi, Device characteristics of CZTSSe thin-film solar cells with 12.6% efficiency, Adv. Energy Mater. 4 (2014) 1301465, https://doi.org/10.1002/aenm.201301465.
[25] O.K. Simya, B.G. Priyadarshini, K. Balachander, A.M. Ashok, Formation of a phase pure kesterite CZTSe thin films using multisource hybrid physical vapour deposition, Mater Res Express 7 (2020) 016419.
[26] T. Ratz, G. Brammertz, R. Caballero, M. León, S. Canulescu, J. Schou, L. Gütay, D. Pareek, T. Taskesen, D.-H. Kim, Physical routes for the synthesis of kesterite, J. Phys. Energy 1 (2019) 042003.
[27] J. Jeon, K.D. Lee, L. Seul Oh, S. Seo, D. Lee, H. Kim, J. Jeong, M.J. Ko, B. Kim, H. J. Son, J.Y. Kim, Highly efficient copper–zinc–tin–selenide (CZTSe) solar cells by electrodeposition, ChemSusChem 7 (2014) 1073–1077, https://doi.org/10.1002/cssc.201301347.
[28] M. Neuschitzer, K. Lienau, M. Guc, L.C. Barrio, S. Haass, J.M. Prieto, Y. Sanchez, M. Espindola-Rodriguez, Y. Romanyuk, A. Perez-Rodriguez, Towards high performance Cd-free CZTSe solar cells with a ZnS (O, OH) buffer layer: the influence of thiourea concentration on chemical bath deposition, J. Phys. D. Appl. Phys. 49 (2016) 125602.
[29] K. Mokurala, L.L. Baranowski, F.W. De Souza Lucas, S. Siol, M.F.A.M. Van Hest, S. Mallick, P. Bhargava, A. Zakutayev, Combinatorial chemical Bath deposition of CdS contacts for chalcogenide photovoltaics, ACS Comb. Sci. 18 (2016) 583–589, https://doi.org/10.1021/acscombsci.6b00074.
[30] S. Sengupta, R. Aggarwal, M. Raula, A review on chemical bath deposition of metal chalcogenide thin films for heterojunction solar cells, J. Mater. Res. 38 (2023) 142–153, https://doi.org/10.1557/s43578-022-00539-9.
[31] K. Tanaka, Y. Fukui, N. Moritake, H. Uchiki, Chemical composition dependence of morphological and optical properties of Cu2ZnSnS4 thin films deposited by sol–gel sulfurization and Cu2ZnSnS4 thin film solar cell efficiency, Sol. Energy Mater. Sol. Cells 95 (2011) 838–842.
[32] L. Chen, H. Deng, J. Tao, W. Zhou, L. Sun, F. Yue, P. Yang, J. Chu, Influence of annealing temperature on structural and optical properties of Cu2MnSnS4 thin films fabricated by sol–gel technique, J. Alloys Compd. 640 (2015) 23–28.
[33] H. Ahmoum, P. Chelvanathan, M.S. Su’ait, M. Boughrara, G. Li, R. Gebauer, K. Sopian, M. Kerouad, N. Amin, Q. Wang, Sol-gel prepared Cu2ZnSnS4 (CZTS) semiconductor thin films: role of solvent removal processing temperature, Mater. Sci. Semicond. Process. 132 (2021) 105874, https://doi.org/10.1016/j.mssp.2021.105874.
[34] J.K. Park, Performance enhancement in powder-fabricated Cu2(ZnSn)Se4 solar cell by roll compression, Materials (2025), https://doi.org/10.3390/MA16031076.
[35] U. Saha, A. Biswas, M.K. Alam, Efficiency enhancement of CZTSe solar cell using CdS (n)/(AgxCu1–x) 2ZnSnSe4 (p)/Cu2ZnSnSe4 (p+) structure, Sol. Energy 221 (2021) 314–322.

[36] Y. Atasoy, E. Bacaksız, A. Çiriş, M.A. Olğar, R. Zan, A.M.J. Al-dala Ali, T. Küçükömeroğlu, B.M. Başol, Improved CZTSe solar cell efficiency via silver and germanium alloying, Sol. Energy 267 (2024) 112247, https://doi.org/10.1016/j.solener.2023.112247.

[37] S. Tao, H. Wang, M. Jia, J. Han, Z. Wu, J. Zhou, M. Baranova, H. Zhu, M. Zhao, D. Zhuang, Ge-doped CZTSe solar cell efficiency beyond 14% by suppressing recombination, Adv. Funct. Mater. 35 (2025) 2423251, https://doi.org/10.1002/adfm.202423251.

[38] A. Chihi, M.F. Boujmil, B. Bessais, Investigation on the performance of CIGS/TiO2 heterojunction using SCAPS software for highly efficient solar cells, J. Elec. Mater. 46 (2017) 5270–5277, https://doi.org/10.1007/s11664-017-5547-0.

[39] C.O. Lawani, G.J. Ibeha, O. Ige, E. Danladi, J.O. Emmanuela, A.J. Ukwenya, P. O. Oyedare, Numerical simulation of copper indium gallium diselenide solar cells using one dimensional SCAPS software, J. Nigerian Soc. Phys. Sci. (2021) 48–58.

[40] S. Souri, M. Marandi, Numerical modelling of the effect of the Ag: ZnSe BSF layer on the high performance of ZnSe/CdTe thin film solar cells by SCAPS-1D software, Opt. Quant. Electron. 55 (2023) 397, https://doi.org/10.1007/s11082-023-04563-9.

[41] Wang, Introduction to Solid State Electronics - Google Scholar. https://scholar.google.com/scholar_lookup?title=Introduction%20to%20Solid%20State%20Electronics&author=F.F.Y.%20Wang&publication_year=1980, 2025 (accessed May 27, 2025).

[42] N. Selmane, A. Cheknane, H.S. Hilal, Optimization of Al-doped ZnO transparent conducting oxide and emitter layers for enhanced performance of Si heterojunction solar cells, J. Elec. Mater. 49 (2020) 2179–2190, https://doi.org/10.1007/s11664-019-07917-w.

[43] R. Bernal-Correa, A. Morales-Acevedo, J. Montes-Monsalve, A. Pulzara-Mora, Design of the TCO (ZnO: Al) thickness for glass/TCO/CdS/CIGS/Mo solar cells, J. Phys. D. Appl. Phys. 49 (2016) 125601.

[44] I. Crupi, S. Boscarino, V. Strano, S. Mirabella, F. Simone, A. Terrasi, Optimization of ZnO: Al/Ag/ZnO: Al structures for ultra-thin high-performance transparent conductive electrodes, Thin Solid Films 520 (2012) 4432–4435.

[45] S. Hamrit, K. Djessas, N. Brihi, B. Viallet, K. Medjnoun, S.E. Grillo, The effect of thickness on the physico-chemical properties of nanostructured ZnO: Al TCO thin films deposited on flexible PEN substrates by RF-magnetron sputtering from a nanopowder target, Ceram. Int. 42 (2016) 16212–16219.

[46] N. Selmane, A. Cheknane, K.M. Gueddouda, F.A. Boukhelkhal, N. Baydogan, M.H. S. Helal, H.S. Hilal, RbGeI3/CuZnSnSSe/CuInGaSe/CdS tandem solar cell with improved performance and lowered cost, J. Mater. Sci. Mater. Electron. 35 (2024) 1109, https://doi.org/10.1007/s10854-024-12889-7.

[47] N. Selmane, A. Cheknane, H.S. Hilal, A new CsPbI2Br/CuZnSnSSe/Si tandem solar cell with higher than 32% efficiency, Micro Nanostruct. 194 (2024) 207940, https://doi.org/10.1016/j.micrna.2024.207940.

[48] C. Emir, A. Tataroglu, U. Gökmen, S.B. Ocak, Analysis of the structural and optical characteristics of ZnSe thin films as interface layer, J. Mater. Sci. Mater. Electron. 36 (2025) 168, https://doi.org/10.1007/s10854-025-14221-3.

[49] N. Selmane, A. Cheknane, M. Aillerie, H.S. Hilal, Effect of ZnO-based TCO on the performance of a-Si H(n)/a-Si H(i)/c-Si H(p)/Al BSF(p+)/Al heterojunction solar cells, Environ. Prog. Sustain. Energy 38 (2019) 13114, https://doi.org/10.1002/ep.13114.

[50] R. Aswathy, K. Mohanan, Microwave assisted synthesis, characterisation and fluorescence studies of some transition metal complexes with a Luminol derivative, J. Fluoresc. 27 (2017) 1–11, https://doi.org/10.1007/s10895-017-2054-x.

[51] Investigating optoelectronic characteristics and improving the efficiency of Mg3AsBr3 perovskite solar cells through machine learning and numerical simulations utilizing diverse charge transport materials, Langmuir (2025), https://doi.org/10.1021/acs.langmuir.5c01821 (accessed September 19, 2025).

[52] A. Ghosh, A.S. Zishan, M. Moumita, Y.A. Kumar, A.K. Roy, S. Islam, S. Ahmed, H. Z. Anonto, A.T. Happy, M. Shameem Ahsan, H.A. Alrafai, A.A. Hassan, Improving the performance of AgCdF3-based perovskite solar cells using machine learning-driven adjustment of active layer and charge transport materials with SCAPS-1D, Inorg. Chem. Commun. 179 (2025) 114829, https://doi.org/10.1016/j.inoche.2025.114829.

[53] A. Ghosh, M.F.I. Buian, M. Maniruzzaman, M. Mahfuz Hossain, A.K. Azad, A. A. Miazee, I. Ragab, A.A. Hassan, H.A. Alrafai, S. Khalaf-Alla Abdelrahim, Numerical analysis and device modelling of a lead-free Sr3PI3/Sr3SbI3 double absorber solar cell for enhanced efficiency, RSC Adv. 14 (2024) 26437–26456, https://doi.org/10.1039/d4ra05079g.

[54] A. Ghosh, M.R. Hasan, M. Moumita, K.U. Apu, S. Begum, A. Rahman, M.A. Bappy, S. Ahmed, Y.A. Kumar, A.A. Hassan, H.A. Alrafai, Discovering the relationship between sulfide and selenide-based HTLs and cubic Ba3SbI3 solar cells with SCAPS-1D and machine learning modelling, Inorg. Chem. Commun. 173 (2025) 113782, https://doi.org/10.1016/j.inoche.2024.113782.

[55] R.H. Sardar, A. Bera, S. Chattopadhyay, S.I. Ali, S. Pramanik, A.C. Mandal, The impact of series (Rs) and shunt resistances (Rsh) on solar cell parameters to enhance the photovoltaic performance of f-PSCs, Opt. Mater. 155 (2024) 115818.

[56] A.D. Dhass, E. Natarajan, L. Ponnusamy, Influence of shunt resistance on the performance of solar photovoltaic cell, in: 2012 International Conference on Emerging Trends in Electrical Engineering and Energy Management (ICETEEEM), IEEE, 2012, pp. 382–386. https://ieeexplore.ieee.org/abstract/document/6494522/ (accessed September 19, 2025).

[57] A. Benisha Chris, S. Pisupati, S. Routray, Performance analysis of CZTSe Kesterite solar cell by adding CZTSSe as BSF layer, J. Phys. Conf. Ser. 2335 (2022) 012040, https://doi.org/10.1088/1742-6596/2335/1/012040.

[58] J. Gulomov, O. Accouche, J. Ziyoitdinov, A. Mirzaalimov, Optimizing CZTSe solar cell architecture: comparative study of ZnO, TiO_2, and MoO_3 as electron transport layers, IEEE Access 12 (2024) 8313–8324, https://doi.org/10.1109/ACCESS.2024.3351675.

[59] H. Ali, A.C. Guler, M. Masar, J. Antos, B. Hanulikova, P. Urbanek, M. Yasir, T. Sopik, M. Machovsky, I. Kuritka, Structural factors influencing photocatalytic and photoelectrochemical performance of low-dimensional ZnO nanostructures, Catal. Today 445 (2024) 115088, https://doi.org/10.1016/j.cattod.2024.115088.

[60] F.-J. Zhang, X. Xiang, J. Yang, Z.-Y. Zhao, The impact of intrinsic point defects on the optoelectronic functionality of CuGaO2: insights from first-principles calculations, Phys. Chem. Chem. Phys. 27 (2025) 5669–5682, https://doi.org/10.1039/D4CP04460F.

[61] H. Yoo, Jun Sung Jang, S.W. Shin, J. Lee, J.-H. Kim, D.M. Kim, I.J. Lee, B.H. Lee, J. Park, J.H. Kim, Influence of the reaction pathway on the defect formation in a Cu2ZnSnSe4 thin film |, ACS Appl. Mater. Interfaces 13 (2021) 13425–13433, https://doi.org/10.1021/acsami.1c01307.

[62] X. Wu, Y. Yuan, Y. Duan, Y. Chen, X. Liu, Improvement of Cu2ZnSnS4 films properties using sulfurized precursor films with Cu-poor/Zn-rich ratio, J. Solid State Chem. 333 (2024) 124641, https://doi.org/10.1016/j.jssc.2024.124641.

[63] D. Li, C. Zeng, W. Xin, G. Zi, R. Hong, Strategies for inhibiting the growth defects of CZTSe thin film, J. Alloys Compd. 1000 (2024) 175105, https://doi.org/10.1016/j.jallcom.2024.175105.

[64] H.A. Nurmi, G. Zenuni, S. Lepikko, R. Saine, M. Vuckovac, R.H.A. Ras, In situ error analysis in contact angle goniometry, Soft Matter 21 (2025) 2422–2429, https://doi.org/10.1039/D4SM01509F.

[65] A. Bhanawat, K. Zhu, L. Pilon, How do bubbles affect light absorption in photoelectrodes for solar water splitting? Sustain. Energy Fuel 6 (2022) 910–924, https://doi.org/10.1039/D1SE01730F.

[66] F. Marchini, C. Chiatti, C. Fabiani, L. Latterini, A. Pisello, Investigating the relationship between surface roughness and reflectance properties of building materials, J. Phys. Conf. Ser. 2685 (2024) 012030, https://doi.org/10.1088/1742-6596/2685/1/012030.

[67] V. Gareyan, Impact of surface roughness on light absorption, Phys. Rev. A 109 (2024) 013515, https://doi.org/10.1103/PhysRevA.109.013515.

[68] J.P.B. van Dam, S.T. Abrahami, A. Yilmaz, Y. Gonzalez-Garcia, H. Terryn, J.M. C. Mol, Effect of surface roughness and chemistry on the adhesion and durability of a steel-epoxy adhesive interface, Int. J. Adhes. Adhes. 96 (2020) 102450, https://doi.org/10.1016/j.ijadhadh.2019.102450.

[69] A. Mortadi, E. El Hafidi, M. Monkade, R. El Moznine, Investigating the influence of absorber layer thickness on the performance of perovskite solar cells: a combined simulation and impedance spectroscopy study, Mater. Sci. Energy Technol. 7 (2024) 158–165, https://doi.org/10.1016/j.mset.2023.10.001.

[70] S.V. Kozodoev, A.I. Muhammad, V.V. Kolos, P.I. Gaiduk, Influence of metal type and layer thickness on absorption of optical radiation by profiled Si3N4/Me/Si3N4 structures, J. Appl. Spectrosc. 92 (2025) 265–270, https://doi.org/10.1007/s10812-025-01906-0.

[71] V. Perraki, Modelling of recombination velocity and doping influence in epitaxial silicon solar cells, Sol. Energy Mater. Sol. Cells 94 (2010) 1597–1603, https://doi.org/10.1016/j.solmat.2010.04.078.

[72] A.H. Oishi, M.T. Anjum, M.M. Islam, M.F. Nayan, Impact of absorber layer thickness on perovskite solar cell efficiency: a performance analysis, Europ. J. Electric. Eng. Comp. Sci. 7 (2023) 48–51.

[73] S. Ashagre, A.K. Ogundele, J.N. Ike, N. Jili, G. Pellicane, K. Zhou, W. Ma, G. T. Mola, Controlling doping concentration of metal nanoparticles for enhanced performance in NFA-based organic solar cell, J. Polym. Sci. 63 (2025) 2199–2208, https://doi.org/10.1002/pol.20250009.

[74] E.A. Nyiekaa, T.A. Aika, E. Danladi, C.E. Akhabue, P.E. Orukpe, Simulation and optimization of 30.17% high performance N-type TCO-free inverted perovskite solar cell using inorganic transport materials, Sci. Rep. 14 (2024) 12024, https://doi.org/10.1038/s41598-024-62882-7.

[75] N.K. Sinha, P. Roy, D.S. Ghosh, A. Khare, Investigation of effect of doping in perovskite solar cells: a numerical simulation approach, Mater Today Proc 83 (2023) 6–13, https://doi.org/10.1016/j.matpr.2022.10.006.

[76] D. Parajuli, D.K. Shah, D. Kc, S. Kumar, M. Park, B. Pant, Influence of doping concentration and thickness of regions on the performance of InGaN single junction-based solar cells: a simulation approach, Electrochem 3 (2022) 407–415, https://doi.org/10.3390/electrochem3030028.

[77] C. Sah, R. Noyce, W. Shockley, Carrier generation and recombination in P-N junctions and P-N junction characteristics, Proc. IRE 45 (1957) 1228–1243, https://doi.org/10.1109/jrproc.1957.278528.

[78] A. Kanevce, T.A. Gessert, Optimizing CdTe solar cell performance: impact of variations in minority-carrier lifetime and carrier density profile, IEEE J. Photovolt. 1 (2011) 99–103, https://doi.org/10.1109/jphotov.2011.2164952.

[79] V.A. Trukhanov, V.V. Bruevich, D.Yu. Paraschuk, Effect of doping on performance of organic solar cells, Phys. Rev. B 84 (2011) 205318, https://doi.org/10.1103/physrevb.84.205318.

[80] K.S. Choe, Simulation on optimum doping levels in Si solar cells, Korean J. Mater. Res. 30 (2020) 509–514, https://doi.org/10.3740/mrsk.2020.30.10.509.

[81] A. Cuevas, Electrons and holes in solar cells with partial rear contacts, Prog. Photovolt. Res. Appl. 22 (2014) 764–774, https://doi.org/10.1002/pip.2433.

[82] F. Atlan, I. Becerril-Romero, S. Giraldo, V. Rotaru, Y. Sánchez, G. Gurieva, S. Schorr, E. Arushanov, A. Pérez-Rodríguez, V. Izquierdo-Roca, M. Guc, Stability of Cu2ZnSnSe4/CdS heterojunction based solar cells under soft post-deposition thermal treatments, Sol. Energy Mater. Sol. Cells 249 (2023) 112046, https://doi.org/10.1016/j.solmat.2022.112046.

[83] D. Nowak, T. Khonsor, D Pareek, **Gütay,**Vapor-Phase Incorporation of Ge in CZTSe Absorbers for Improved Stability of High-Efficiency Kesterite Solar Cells, Appl. Sci. 12 (2025) 1376, https://doi.org/10.3390/app12031376.

[84] K. Yu, E.A. Carter, A strategy to stabilize Kesterite CZTS for high-performance solar cells, Chem. Mater. 27 (2015) 2920–2927, https://doi.org/10.1021/acs.chemmater.5b00172.
[85] Md.S. Reza, A. Ghosh, Md.S. Reza, S. Sultana, N.S. Awwad, H.A. Alturaifi, Strategic design and evaluation of charge transport layers for high-efficiency lead-free BeSiP2-based perovskite solar cells: a careful examination into electron and hole transport layers, Sol. Energy 287 (2025) 113210, https://doi.org/10.1016/j.solener.2024.113210.
[86] T. Pansuriya, R. Malani, V. Kheraj, Investigations on the effect of buffer layer on CMTS based thin film solar cell using SCAPS 1-D, Opt. Mater. 126 (2022) 112150, https://doi.org/10.1016/j.optmat.2022.112150.
[87] J. El Hamdaoui, M. El-Yadri, K. Lakaal, M. Kria, M. Courel, M. Ojeda, L.M. Pérez, D. Laroze, E. Feddi, Ab initio study on electronic and optical properties of Cu2NiGeS4 for photovoltaic applications, Sol. Energy 237 (2022) 333–339, https://doi.org/10.1016/j.solener.2022.03.052.
[88] B.F. Afrah, S. Naceur, C. Ali, K. Fakhereddine, H. Bsharat, H.S. Hilal, Cost-lowering and performance-improvement of B-γ-CsSnI3 solar cells by adding CZTSSe absorber, J. Electroanal. Chem. 996 (2025) 119369, https://doi.org/10.1016/j.jelechem.2025.119369.
[89] D. Cozza, C.M. Ruiz, D. Duché, J.J. Simon, L. Escoubas, Modeling the back contact of Cu2ZnSnSe4 solar cells, IEEE J. Photovolt. 6 (2016) 1292–1297, https://doi.org/10.1109/JPHOTOV.2016.2576678.